JACS
JOURNAL OF THE AMERICAN CHEMICAL SOCIETY

Article

pubs.acs.org/JACS

Experimental and Computational Studies of the Neutral and Reduced States of Indeno[1,2-*b*]fluorene

Bradley D. Rose,[†] Natalie J. Sumner,[‡] Alexander S. Filatov,[‡] Steven J. Peters,[∥] Lev N. Zakharov,[§] Marina A. Petrukhina,[‡] and Michael M. Haley*[,†]

[†]Department of Chemistry & Biochemistry and Materials Science Institute, University of Oregon, Eugene, Oregon 97403-1253, United States

[‡]Department of Chemistry, University at Albany, State University of New York, Albany, New York 12222-0100, United States

[∥]Department of Chemistry, Illinois State University, Normal, Illinois 61790-4160, United States

[§]CAMCOR, University of Oregon, Eugene, Oregon 97403, United States

Supporting Information

ABSTRACT: This study examines the intrinsic structural and optoelectronic properties of the neutral indeno[1,2-*b*]fluorene skeleton as well as those of the corresponding anion radical and dianion. We report their characterization by analysis of solid-state structures and EPR, NMR, and absorbance spectra. Additionally, 20 popular density functional theory methods are used to evaluate their performance for predicting NMR chemical shifts, EPR hyperfine coupling constants, and low-energy transitions of the absorbance spectrum to act as a guide for future studies. This information can be used for a better understanding and tuning of the electron-transporting/accepting ability of the indenofluorene core for use in organic photovoltaics and organic field effect transistors.

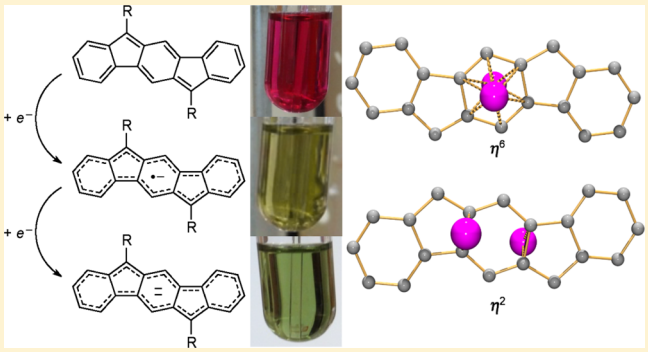

INTRODUCTION

Polycyclic conjugated hydrocarbons (PCHs) have intrigued chemists for decades because of their interesting and varied physical properties, which result from the specific electronic structure of each unique scaffold.[1] Renewed interest in the optical and magnetic properties of PCHs in recent years has arisen from their applications as electronic materials in devices,[2] due to the fact that charge is transported more easily through π orbitals as compared to their exclusively σ-bonded counterparts. A driving force for research into organic electronics is the need to develop materials for use in inexpensive electronic devices that are easily mass-produced, for example, by roll-to-roll printing.[3] One widely studied, π-electron-rich compound is pentacene (**1**, Figure 1). This molecule and its numerous derivatives display relatively high performance in organic field effect transistors (OFETs) and organic photovoltaics (OPVs).[3] The larger acenes, however, are inherently prone to degradation via cycloaddition pathways of the "locked" *s-cis*-diene(s) within the acene core.

A tremendous variety of additional π-electron-rich motifs (Figure 1) have been explored over the past decade, such as larger condensed aromatics (e.g., hexabenzocoronene, **2**),[4] heteroatomic acenes (e.g., **3**),[5] and heteroatomic acene-like structures (e.g., **4**).[6] It is worth noting that, in the last example (**4**), one or more of the six-membered rings was replaced with a five-membered heterocycle. Only recently has this same modification been examined for five-membered carbocycles; the most prevalent examples are molecules based on benzo- and dibenzopentalenes (e.g., **5**).[7] Studies have shown that a vast majority of these new PCH structures are electron-donating and thus exhibit p-type semiconducting behavior in devices. Far fewer molecules are electron-accepting and thus exhibit n-type semiconducting behavior in devices; therefore, there is need to develop new organic molecules that possess electron-accepting properties so that they are available in the toolbox of materials chemists.

A PCH scaffold that is structurally similar to pentacene is indeno[1,2-*b*]fluorene (IF, **6**).[8] Replacement of two six-membered rings in **1** with five-membered carbocycles means two fewer π-electrons and thus a formally anti-aromatic 20 π-electron skeleton. This class of hydrocarbons has been rarely studied; prior to 2011, the four known examples were either unstable or poorly characterized.[9,10] Such instability might be anticipated since *s*-indacene, a molecule too reactive to be isolated, is a structural subunit of the IF scaffold; however, *s*-indacene could be kinetically stabilized by inclusion of four *tert*-butyl groups (e.g., **7**).[11]

Over the past three years our group[12−15] and others[16] have developed or adapted synthetic methods that permit the

Received: April 17, 2014
Published: May 30, 2014

   dx.doi.org/10.1021/ja503870z | *J. Am. Chem. Soc.* 2014, 136, 9181−9189

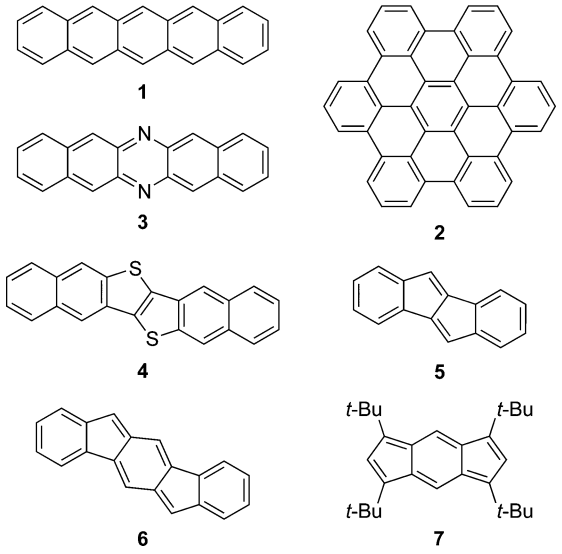

Figure 1. Representative examples of π-electron-rich polycyclic conjugated hydrocarbons.

preparation of indeno[1,2-*b*]fluorene derivatives on the gram scale, which in turn should allow IFs to be further explored for use as organic electronic materials.[14,15] A key discovery in our research has been the high electron affinity that is inherent to the IF scaffold, a result of the inclusion of the five-membered carbocycles. A simple explanation for the ease of reduction is that, upon accepting two extra electrons, both five-membered rings become aromatic and a 22 π-electron species is generated. In a similar manner, *s*-indacene **7** could be reduced and the resultant anion radical[17] and dianion[18] characterized. This information is useful to detail the electron-accepting and/or -transporting behavior of an organic material. To this end we sought to characterize the reduced states of the IF scaffold to determine the location and effects on the molecular structure. This in turn should afford better insight and understanding when designing materials for electron-transporting and/or -accepting applications, as the phase and overlap of the relevant molecular orbitals are critically important for applications in devices.[19]

One goal in the design of new organic materials is to be able to easily screen possible structures using computational methods to find molecules predicted to have a desirable property or properties.[20] Density functional theory (DFT) has opened the door for routine calculations to be completed in the time frame of a few days on desktop computers to inexpensively probe some of the basic properties that influence whether or not a compound is worthy of synthesis; however, with the plethora of DFT methods available, we decided to obtain data for a model electron-accepting PCH, i.e., **6**. We wanted to find a method that gives reasonable results and is accessible to a broad audience. This inherently excludes very specialized techniques or complicated correlations and very high levels of theory, since many systems of interest consist of dozens of atoms. With that in mind, the limiting factors are that we wanted (1) to utilize readily available DFT methods, (2) minimal manipulation of data, and (3) methods that can be easily applied by using a desktop computer with minimal training.

There are numerous benchmark studies for DFT as well as other post-Hartree−Fock methods. Some well-known examples include atomization energies, enthalpies of reactions, ligand binding energies, ionization potentials, and electron affinities, to name a few.[21,22] We sought to assess a selection of DFT methods on the basis of spectroscopic properties. Considerable theoretical groundwork has been done to enable the "routine" computation of these spectral parameters, and somewhat surprisingly there lacks, to the best of our knowledge, a broad assessment of DFT functionals for the prediction of NMR chemical shifts of neutral and the more difficult case of charged states.[23−25] Likewise, most of the studies exploring DFT prediction of isotropic hyperfine coupling constants (HFCC) for free radicals survey few DFT methods.[26,27] Studies have also been performed that explore the energies predicted by time-dependent DFT (TD-DFT); however, none have examined the predictions for reduced PCHs.[22,28,29] This current study is not a comprehensive test bed consisting of dozens of molecules, but instead we use it as an entry point for investigating the feasibility for PCHs and their negatively charged species, which is important for the development of electron-accepting and/or -transporting materials from theory.

Herein we report the formation and characterization of the accessible redox states of 6,12-bis[(trialkylsilyl)ethynyl]indeno-[1,2-*b*]fluorenes **6a** and **6b**. The IF scaffold is convenient for this study since there are no major geometric or symmetry changes for the different redox states, as is the case in, for example, cyclooctatetraene.[30] We compare the experimental data with those derived for computational analogue **6c** utilizing 20 DFT methods to determine their performance for predicting spectroscopic properties for the states considered. The functionals are evaluated by calculating the ^{1}H and ^{13}C NMR spectra of neutral **6c** and its corresponding dianion, the HFCCs for the anion radical, and the low-energy transitions in the absorbance spectra of the neutral molecule, anion radical, and dianion. To our knowledge this study represents one of the first broad assessments comparing the predictive properties of varying DFT methods for differing redox states of a PCH.

EXPERIMENTAL SECTION

IF derivatives **6a** and **6b** were synthesized by previously reported procedures.[13,14] The EPR spectrum of the anion radical $\mathbf{6a}^{\bullet-}$ was obtained by reducing the neutral compound with 1 equiv of K in THF to give the light yellow anion radical (Scheme 1), in contrast to the deep purple color of **6a**. The NMR spectrum of the dark green solution of the dianion was obtained by reducing **6a** with 2 equiv of K in the presence of 18-crown-6 to help solubilize $\mathbf{6a}^{2-}$. The absorbance spectra were obtained by controlled reduction of **6a** in THF with K in the presence of 18-crown-6 in a quartz cuvette sealed with a screw cap. Single crystals of dianion $\mathbf{6b}^{2-}$ were prepared by reduction in THF with excess Rb in the presence of 18-crown-6; see the Supporting Information for complete experimental details.

The DFT functionals utilized in this study were chosen from a variety of ones that are readily available and popular in the literature, i.e., the 2012 DFT poll list.[31] The functionals considered are the generalized gradient approximation (GGA) functionals BP86,[32,33] BLYP,[32] PBE,[34] and PW91.[35] The hybrid GGA functionals used are BHandHLYP,[36] B3PW91,[37] B3LYP,[38] HSE06,[39−41] PBE0,[42−44] and mPW1PW91.[45] The hybrid meta GGA functionals used are M06,[46] M06-2X,[46] M06-L,[47] M05,[48] M05-2X,[49] and τ-HCTH.[50] Dispersion-corrected functionals used are B97-D[51] and ωB97X-D.[52,53] Range-separated functionals used are LC-ωPBE[54−56] and CAM-B3LYP.[57] Hartree−Fock (HF) provides a reference as a simple *ab initio* method alongside the DFT methods. All calculations were restricted to C_2 symmetry, and positions will only be referred to by the lowest numbering with the knowledge that it also refers to the other symmetrically equivalent position. These methods were used as implemented in Gaussian 09, Revision C.01,[58] and all calculations were done for the gas-phase molecules. For computational ease the

Scheme 1. Synthesis of Indeno[1,2-*b*]fluorene Anion Radical ($6a^{\bullet-}$) and Dianion ($6a,b^{2-}$)[a]

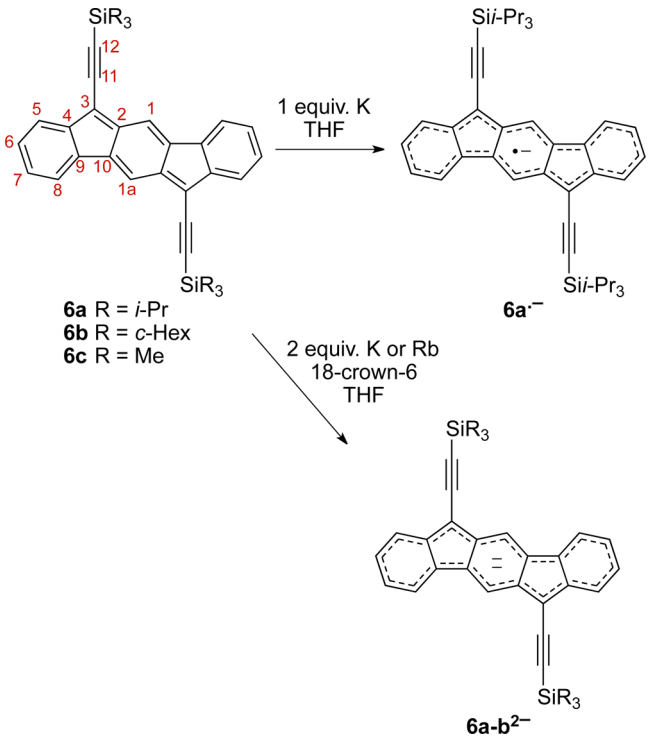

[a]The atom numbering scheme used herein is shown in red.

trialkylsilyl groups of **6a,b** were truncated as a trimethylsilyl group (**6c**) since we have shown previously that altering the trialkylsilyl functionality has very little effect on the electronics, which are dominated by the π system.[59]

RESULTS AND DISCUSSION

Experimental and Calculated Structures for the Neutral and Dianion IF 6. Single crystals of **6a** suitable for X-ray diffraction study were obtained from $CHCl_3$; the molecular structure and crystal packing are shown in Figure 2. The bond lengths, along with those previously reported for the structure of **6b**,[60] are compiled in Table 1. Unlike most other bisethynylated IF derivatives,[8] both **6a** and **6b** pack in such a way that the bulky trialkylsilyl groups are situated over the IF core unit of neighboring molecules (CH···π contacts start at ca. 2.69 Å), effectively preventing any π–π stacking within the crystal lattice (closest π–π contacts >3.7 Å).

Fortunately, we were able to obtain single crystals suitable for X-ray diffraction of dianion $\mathbf{6b}^{2-}$ via reduction with Rb in the presence of 18-crown-6, whereas analogous reaction conditions did not afford suitable crystals of $\mathbf{6a}^{2-}$. As depicted in Figure 3, two crystallographically independent molecules were found in the solved structure, where the two Rb atoms exhibit either η^6-coordination (left) or η^2-coordination (right), illustrating flexibility of the dianion in alkali metal binding.

A close-up view of the indenofluorene core of $\mathbf{6b}^{2-}$ with the alkynes and crown ethers removed (Figure 4, Table 1) clearly shows the two different coordination motifs, where both Rb^+ cations are either η^6-coordinated to the central six-membered ring (3.216(7)–3.370(7) Å) or side-coordinated on opposite ends of the central six-membered ring (3.048(6)–3.133(6) Å) with additional longer contacts to the adjacent C-atoms of five- and six-membered rings (3.364(6)–3.637(7) Å). The corresponding Rb···C distances are comparable with those measured in the π-adducts of Rb(I) with planar and nonplanar polyaromatic hydrocarbons.[61−63] The differences in the X-ray-determined bond lengths between the η^2 and η^6 isomers of $\mathbf{6b}^{2-}$ are minimal and lie below the error in the data. In contrast, the X-ray structure of the $[(K^+)_2(18\text{-crown-}6)_2]$ complex of $\mathbf{7}^{2-}$ shows the alkali metals to be η^5-coordinated to the five-membered rings;[18] however, η^6-coordination is observed in the $[(K^+)(18\text{-crown-}6)]$ complex of fluorenyl anion, so this motif has precedence.[64]

In the solid-state structure, additional intramolecular interactions can be identified between the crown ether and the planar surface of the dianion. In the case of η^2-bound complex, short CH···π contacts are observed with the five-membered rings (2.379(9) Å to the centroid of the five-

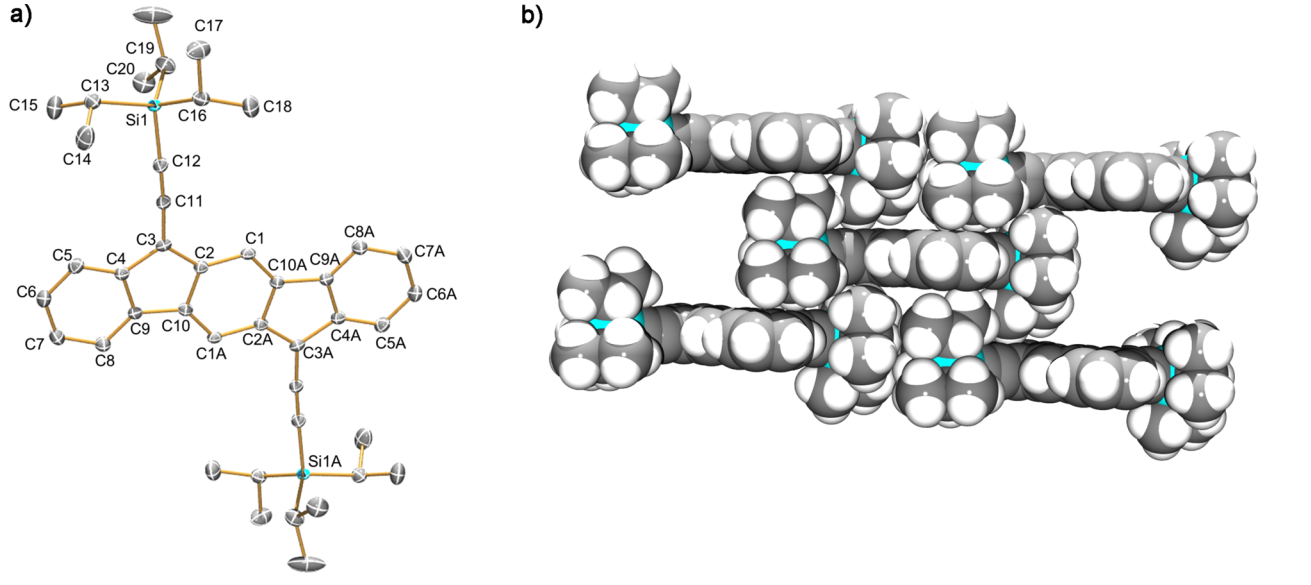

Figure 2. Molecular structure (left) and crystal packing (right) of IF **6a**. Hydrogen atoms in the molecular structure are omitted for clarity. Ellipsoids are drawn at the 30% probability level.

dx.doi.org/10.1021/ja503870z | *J. Am. Chem. Soc.* 2014, 136, 9181–9189

Table 1. Comparison of the Bond Distances (Å) of 6a, 6b, and $6b^{2-}$ from X-ray Data and B3LYP/6-31++G(d,p) Calculated Structures of 6c, $6c^{\bullet-}$, and $6c^{2-}$

	neutral					radical anion	dianion				
	X-ray						X-ray				
bond	**6a**	**6b**	avg	calcd	UE	calcd	η^6	η^2	avg	calcd	UE
1-10a	1.354(6)	1.364(5)	1.359	1.369	0.010	1.387	1.386(9)	1.391(9)	1.389	1.401	0.013
1-2	1.424(6)	1.423(5)	1.424	1.428	0.004	1.412	1.396(9)	1.392(9)	1.394	1.402	0.008
2-3	1.382(6)	1.395(5)	1.389	1.399	0.011	1.431	1.439(9)	1.407(9)	1.423	1.459	0.036
3-4	1.472(6)	1.469(5)	1.471	1.468	0.002	1.452	1.414(9)	1.446(9)	1.430	1.439	0.009
4-5	1.379(6)	1.372(5)	1.376	1.392	0.016	1.403	1.394(9)	1.405(10)	1.400	1.399	0.000
5-6	1.384(6)	1.394(5)	1.389	1.400	0.011	1.397	1.369(9)	1.380(10)	1.375	1.396	0.022
6-7	1.374(7)	1.370(5)	1.372	1.401	0.029	1.408	1.397(9)	1.413(9)	1.405	1.412	0.007
7-8	1.389(6)	1.394(5)	1.392	1.403	0.012	1.399	1.387(9)	1.367(9)	1.377	1.401	0.024
8-9	1.373(6)	1.370(5)	1.372	1.392	0.020	1.397	1.392(8)	1.388(9)	1.390	1.399	0.009
9-10	1.481(6)	1.465(5)	1.473	1.467	0.006	1.458	1.439(9)	1.449(9)	1.444	1.453	0.009
4-9	1.410(6)	1.406(5)	1.408	1.422	0.014	1.432	1.434(9)	1.433(9)	1.434	1.443	0.010
2-10	1.456(5)	1.437(5)	1.447	1.458	0.012	1.447	1.442(9)	1.454(9)	1.448	1.442	0.006
3-11	1.411(6)	1.411(5)	1.411	1.407	0.004	1.398	1.441(10)	1.425(10)	1.433	1.385	0.048
11-12	1.206(6)	1.211(5)	1.209	1.227	0.019	1.234	1.210(9)	1.220(9)	1.215	1.245	0.030
12-Si	1.843(4)	1.845(4)	1.844	1.846	0.002	1.816	1.821(8)	1.821(8)	1.821	1.786	0.035
MUE					0.011						0.018

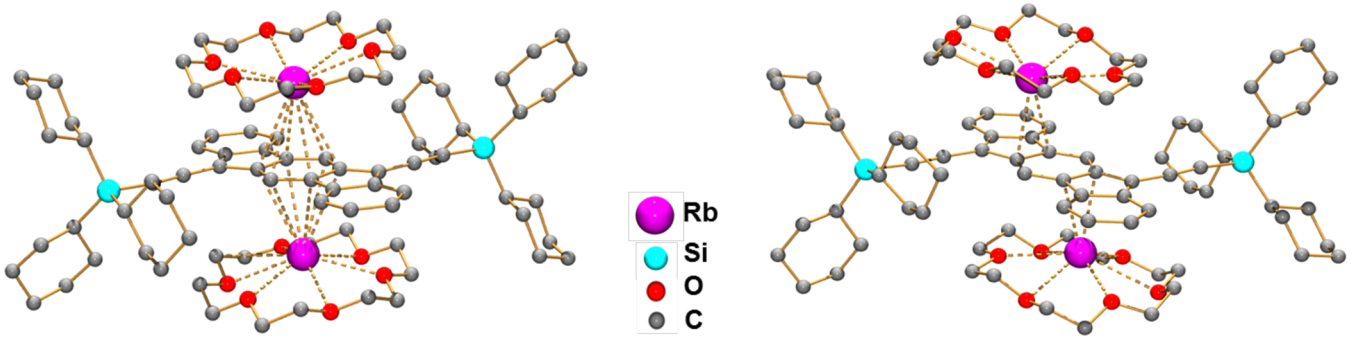

Figure 3. Molecular structure of $6b^{2-}$ exhibiting η^6-coordination (left) and η^2-coordination (right) of the Rb^+ cations. Hydrogen atoms are omitted for clarity. The same atom color-coding scheme is used in Figure 4.

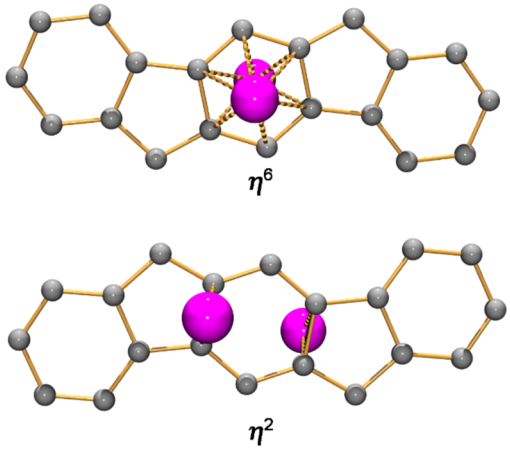

Figure 4. Close-up view of indenofluorene core of $6b^{2-}$ with both Rb^+ ions either (top) η^6-coordinated to the central six-membered ring or (bottom) η^2-side-coordinated to the central six-membered ring.

membered ring). Slightly longer CH···π contacts are found with the peripheral benzene rings of the η^6-bound complex (2.706(9) Å to the centroid of the six-membered ring). While alkali metal cations are generally considered to be good electrostatic probes of electron density distribution over the hydrocarbon surface,[65−67] the crown ether interactions with the π-system also play a crucial role and may be responsible for specific positioning of the cationic units over the negatively charged hydrocarbon surfaces.[62,68] The observation of two different coordination modes in $6b^{2-}$ is a result of such interplay between Rb^+···π and CH···π interactions with the negatively charged surface of the indenofluorene core. The calculated electrostatic potential map (Figure S5) corroborates the experimental findings, in that the greatest charge density of the dianion is found in the central six-membered ring.

Unlike the structure of **7**, which was discovered to be a rare example of a nonalternant (i.e., delocalized) anti-aromatic compound,[69] benzo-fusion to the indacene core affords the alternant *p*-xylylene motif found experimentally (X-ray) and reproduced computationally (B3LYP) in the indeno[1,2-*b*]fluorenes.[12,13,15] Typically, bonds 1-10a and 2-3 are short (1.35−1.39 Å) and bond 1-2 is long (1.42−1.43 Å). Upon 2-fold reduction of **6b**, the lengths of bonds 1-2 and 1-10a in $6b^{2-}$ become nearly homogeneous (1.386−1.396 Å), suggesting regeneration of a benzenoid configuration within the central six-membered ring. In addition, bond 2-3 is lengthened and bonds 3-4 and 9-10 are significantly shortened, implicating the formation of a cyclopentadiene-like aromatic anion in each five-membered ring. As a result, the entire hydrocarbon now obeys Hückel's rule with a total of 22 π-electrons within the

dx.doi.org/10.1021/ja503870z | J. Am. Chem. Soc. 2014, 136, 9181−9189

pentacyclic structure. In comparison, the geometrical changes upon reduction of **7** to $\mathbf{7}^{2-}$ were much more modest, where the bridging bond (bond 2-10 in the case of **6**) increased by 0.023 Å and all other bond lengths possessed differences less than 0.011 Å;[18,68] the length of bond 2-10 is essentially unchanged in the case for **6b** to $\mathbf{6b}^{2-}$. Notably, the planarity of the ligand skeleton has not changed upon addition of 2 electrons and binding of Rb^+ ions. The average deviation of C-atoms from the least-squares plane passing through all atoms of the ligand is less than 0.02 Å in both the neutral and charged states.

For the broader picture of this study, comparison of the bond lengths in the X-ray data and the gas-phase computed structures in Table 1 reveals no notable discrepancies, and as expected, packing forces slightly alter the bond lengths from the gas-phase calculated structures. IFs **6a**,**b** demonstrate the effects of the packing forces have on the scaffold, with the largest effected bond difference of 0.019 Å for the 2-10 bond. In comparison, the largest error discrepancy between the calculated structure and the X-ray data for the neutral molecule is 0.029 Å, with a mean unsigned error (MUE) of 0.011 Å. The calculated structure of $\mathbf{6c}^{2-}$ omitted explicit inclusion of the metal, and for comparison with $\mathbf{6b}^{2-}$, the largest discrepancy is 0.048 Å, with a MUE of 0.018 Å. The low MUE indicates that the geometries determined using B3LYP/6-31++G(d,p) are reasonable for further use in this study; previous studies have also shown that B3LYP yields reasonable results for similar charged systems.[70]

EPR Spectrum of Anion Radical $\mathbf{6a}^{\bullet-}$. To probe the location of the electron density within an IF skeleton that is reduced with a single electron, we generated and characterized the anion radical $\mathbf{6a}^{\bullet-}$. Upon single-electron reduction with K, the color of the solution changed from the deep purple of **6a** to a clear yellow of $\mathbf{6a}^{\bullet-}$. The experimental EPR spectrum of $\mathbf{6a}^{\bullet-}$ along with the simulated spectrum are shown in Figure 5; the hyperfine coupling present in the EPR spectrum was simulated with the EasySpin[71] package utilizing MATLAB code.[72] The close agreement between simulation and experiment is demonstrated by an R^2 value of 0.987. Interestingly, when the reduction was attempted using HMPA as the solvent, **6a** was reduced to $\mathbf{6a}^{\bullet-}$ by the HMPA as it was distilled into the apparatus, illustrating the high electron affinity of **6a**.

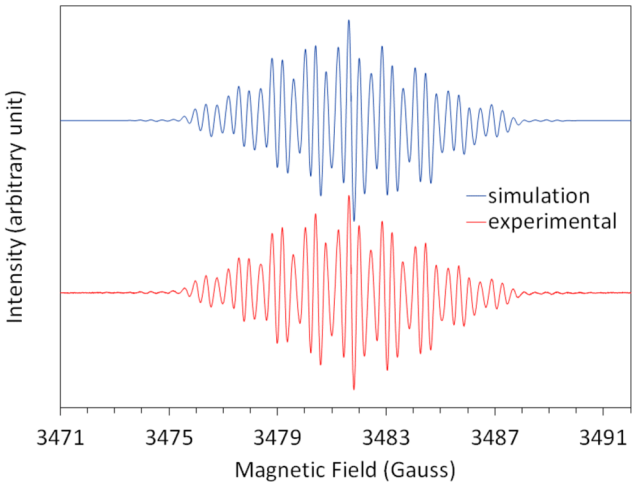

Figure 5. Experimental and simulated EPR spectra of $\mathbf{6a}^{\bullet-}$, using two of each of the HFCCs listed in Table 2.

We next compared the experimental hyperfine coupling constants (HFCCs) of $\mathbf{6a}^{\bullet-}$ with calculated values for $\mathbf{6c}^{\bullet-}$ to assess the ability of various DFT functionals to determine these numbers. The geometry used for calculating HFCCs was optimized using UB3LYP/6-31++G(d,p). Single-point energies were then calculated with each method using a relatively large 6-311++G(2df,2pd) balanced Pople basis set of triple zeta quality and diffuse functions on all atoms, since it is known that the HFCC is critically dependent on the description of the Kohn−Sham wave function close to the nucleus and the size of the basis set.[73] The absolute sign of the HFCCs was not experimentally determined, but for comparison purposes the sign was assumed to be the same as that of the calculated value. The MUE and mean signed error (MSE) were used for analyzing the agreement between the computed values and experimentally determined values. The data reveal the three best-performing functionals were B3PW91, B3LYP, and B97-D, with several others performing quite well. It is also clear that HF does a poor job describing the HFCCs for this hydrocarbon.

Unfortunately, there are many sites on $\mathbf{6a}^{\bullet-}$ that are not measurable using EPR due to the relatively few spin-active nuclei acting as electron density probes around the scaffold. Nevertheless, the location of the spin densities for the measured sites can be used to determine the unpaired electrons' spin density in parts of the π-system. Experimental spin densities can be determined by applying the McConnell equation,

$$a_X = Q\rho_X \quad (1)$$

where the experimental HFCC (a_X) is related to the spin density (ρ_X) using the proportionality factor (Q). Using Q_H = 24.2 and Q_{Si} = 24.4 was found to give spin densities that are in reasonable agreement with the B3PW91 results, as shown in Table 2. This good agreement lends credence to the use of the B3PW91 method as a computational tool to evaluate spin density. The resulting spin density plot (Figure 6) reveals that the spin density has slightly higher density on the central indacene motif and on the ethynyl π-system than the peripheral benzene rings. Interestingly, this is consistent with the Rb-binding sites observed also in the X-ray crystal structure of $\mathbf{6b}^{2-}$. The LUMO density map of the neutral species is nearly identical to the SOMO density plot and slightly reminiscent of the spin density plot, and thus seems a reasonable first approximation to the location of the unpaired electron as shown in Figure 6.

Table 2. Spin Densities of $\mathbf{6a}^{\bullet-}$ (ρ_C) as Related to the Experimental HFCC (a_H) and DFT Calculated Values of $\mathbf{6c}^{\bullet-}$

position	a_X	Q	ρ_C	B3PW91 Mulliken spin density
1	2.48[a]	24.2	0.102	0.101
5	1.26[a]	24.2	0.052	0.052
6	0.37[a]	24.2	0.015	−0.027
7	1.53[a]	24.2	0.063	0.070
8	0.40[a]	24.2	0.017	−0.029
12	4.05[b]	24.4	0.166	0.166

[a] a_H. [b] a_{Si}.

NMR Spectra of Neutral and Dianion IF 6. We successfully obtained ^1H and ^{13}C NMR data for dianion $\mathbf{6a}^{2-}$, which was generated by reduction of **6a** with K in THF-d_8 in

dx.doi.org/10.1021/ja503870z | J. Am. Chem. Soc. 2014, 136, 9181−9189

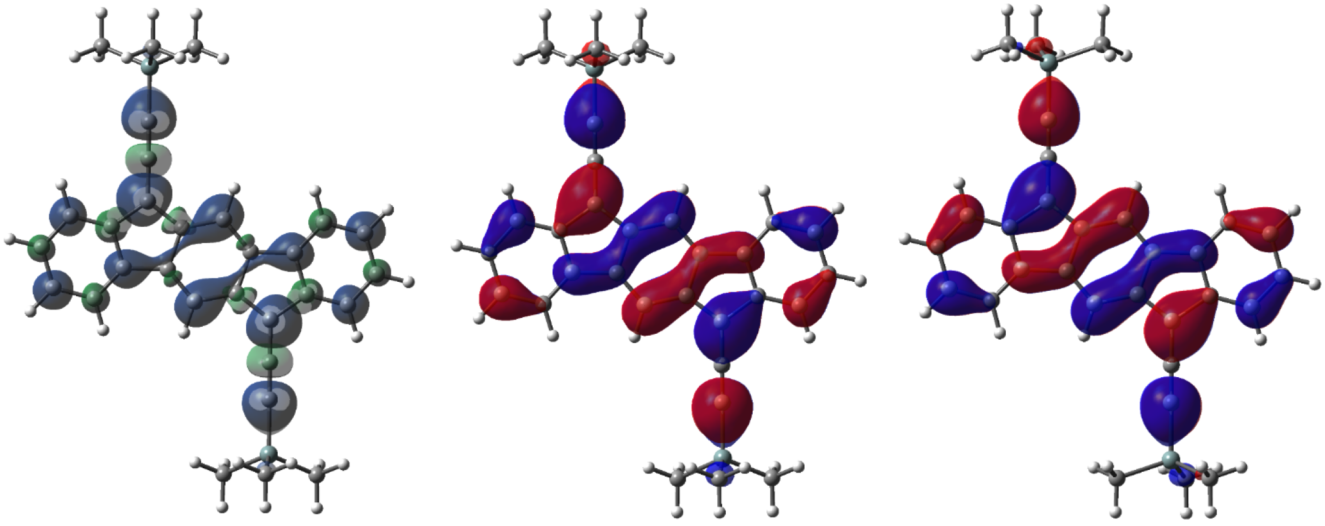

Figure 6. B3PW91 spin density plot (left) and SOMO density plot (center) for $\mathbf{6c}^{\bullet-}$ and LUMO density plot (right) for **6c**.

the presence of 18-crown-6. Comparison of the methine protons of the neutral species to those in the dianion (Figure 7)

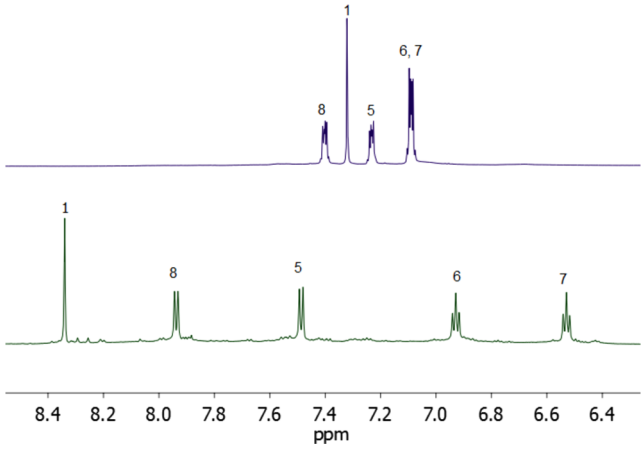

Figure 7. Partial ^{1}H NMR spectra of the methine protons of neutral **6a** (top) and dianion $\mathbf{6a}^{2-}$ (bottom) in THF-d_8, with assigned hydrogen position listed above peaks.

clearly shows that the most affected hydrogen atom is located on position 1. The deshielded hydrogen shifts downfield by ca. 1 ppm, which is indicative of the newly introduced diatropic ring current that results from the addition of two electrons to make a 22 π-electron species. An even greater downfield shift of the analogous protons was observed upon reduction of **7** to $\mathbf{7}^{2-}$ ($\Delta\delta$ ~1.4 ppm).[18] This diatropic ring current also deshields H8 and H5 upon two-electron reduction from **6a** to $\mathbf{6a}^{2-}$, as indicated by ca. 0.5 and 0.3 ppm shifts downfield, respectively. In contrast, H6 and H7 become shielded and shift upfield by 0.2 and 0.6 ppm, respectively.

As one might expect, most of the ^{13}C NMR peaks of $\mathbf{6a}^{2-}$ are significantly shielded in comparison to the corresponding peaks in **6a**, attributable to the increased electron density (Tables S6 and S7). This effect is most evident in carbon 3 of the pentacyclic skeleton, which shifts upfield by more than 50 ppm, suggesting considerable anionic character. Interestingly, alkyne carbons 11 and 12 are deshielded ($\Delta\delta$ ~23.5 ppm) and shielded ($\Delta\delta$ ~21.4 ppm), respectively, suggesting some delocalization of the negative charge out onto C12 that could be stabilized by the α-silicon atom; however, the solid-state data for both the η^2 and η^6 isomers of $\mathbf{6b}^{2-}$ indicate such a contribution is minimal.

To further test the DFT functionals under consideration, we calculated the ^{1}H and ^{13}C NMR chemical shifts and compared them with the experimental data. Since the structure in question is a PCH, solvent effects should have minimal influence on the NMR chemical shifts.[13] The geometry of $\mathbf{6c}^{2-}$ was minimized using RB3LYP/6-31++G(d,p), and values were referenced to tetramethylsilane (0 ppm) using the same method. Here again, in order to minimize basis set effects, the relatively large 6-311++G(2df,2pd) basis set was used to assess the various methods without having to worry about fortuitous error cancellation that might occur with a smaller basis set. The calculations were performed using the Gauge-Independent Atomic Orbital (GIAO) method, and the complete data are compiled in Tables S4–S7.

The computational data clearly show there are several methods that perform well in predicting the chemical shift of the ^{1}H NMR spectrum. Notably, B3LYP, PBE, PW91, and BP86 had MSEs and MUEs within 0.1 ppm of the measured ^{1}H chemical shifts for both the dianion and neutral compound. The ^{13}C NMR spectral prediction had three functionals with MSE and MUE below 5 ppm—B3LYP, B97-D, and τ-HCTH. Interestingly, in both cases, if a functional did a poor job predicting the chemical shift of the neutral species, it typically performed equally poorly for predicting the dianion data, and vice versa.

Unfortunately, unambiguous assignment of the ^{13}C NMR spectrum was not possible when interpreting COSY, HSQC, and HMBC spectra. This is due to the carbons located on the cyclopentadiene moiety lacking spin-active nuclei to assist with clear interpretation. The lack of definitive NMR spectral assignment and little data comparing many readily available DFT methods for assisting with NMR spectral assignment provided partial motivation for the undertaking of this study.

Electronic Absorption Spectra. As a final test we examined the electronic absorption spectra of the neutral, anion radical, and dianion of IF **6a**, as these should serve as representative spectroscopic handles for the reduced molecule in electronic devices such as OPVs.[74] Experimental data were gathered by reducing **6a** with potassium in a cuvette and

dx.doi.org/10.1021/ja503870z | J. Am. Chem. Soc. 2014, 136, 9181–9189

monitoring the progress via absorbance spectrum from the UV to the near-infrared (NIR), as shown in Figure 8. The reduction

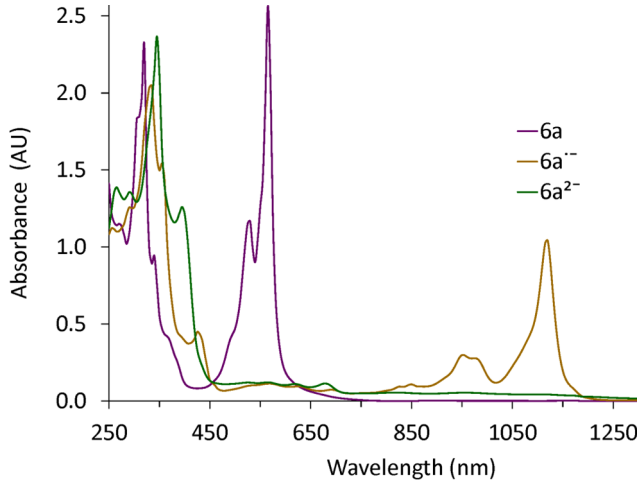

Figure 8. Electronic absorption spectra of **6a**, **6a**$^{\bullet-}$, and **6a**$^{2-}$.

state was a visual feast, as the starting purple color of **6a** faded upon exposure to K to the light yellow of **6a**$^{\bullet-}$ and then to the light green of **6a**$^{2-}$. The green hue of the dianion suggests that the weak peak at ca. 500−700 nm is likely responsible for this transition. The absorbance spectrum shows vibronic coupling for the lowest energy transition, indicative of a small geometry change upon excitation.[75]

Again, the DFT functionals were assessed in terms of their ability to predict the low-energy electronics transitions using the model system of **6c**, **6c**$^{\bullet-}$, and **6c**$^{2-}$ (Table S8). TD-DFT calculations were performed omitting Franck−Condon effects. The exclusion of Franck−Condon effects will cause the spectra for low-energy transitions to be incorrectly modeled, as vibronic effects clearly play an important role; thus, no attempt was made to assess the absorbance spectral prediction for the UV to the NIR, and instead only the energy of the lowest energy transition was assessed.[29,76] The distribution of the vibronic coupling indicates that the lowest energy peak is likely the 0-0 peak, which thus will be used as an estimate for comparison with the calculated vertical excitation energy.[75]

In predicting the lowest energy transition in general, the functionals performed somewhat similarly for the neutral compound. A notable point is that the time-dependent calculations on **6c** find a triplet that is slightly lower in energy than the closed-shell solution, contrary to experiment, for HF, BHandHLYP, PBE0, HSE06, LC-ωPBE, CAM-B3LYP, M05-2X, M05, M06, ωB97X-D, and mPW1PW91. The lowest energy transition for the neutral molecule via ωB97X-D, CAM-B3LYP, BHandHLYP, M05-2X, and M06-2X was found to be within 0.1 eV of the experimental value, and for the anion radical CAM-B3LYP, BHandHLYP, M05, and ωB97X-D gave transition energies that differed by less than 0.1 eV from experiment.

The dianion proved to be a very challenging case for nearly all functionals, with results varying significantly. Some of the results were without clear interpretation, so in cases where there were two absorbance energies that had similarly large oscillator strengths, both are listed, and this is denoted by parentheses and a number following the functionals that possessed this problem. From the data in Table S8, it is clear that mPW1PW91 (2), M05 (2), B3PW91 (2), M05 (1), B3PW91 (1), and HSE06 (2) gave results within 0.1 eV of the experimental values, but with ambiguity. The only functional that gave one result within 0.1 eV of the experimental value was PBE0.

CONCLUSIONS

We have synthesized and characterized derivatives of **6**, **6**$^{\bullet-}$, and **6**$^{2-}$ to explore the structure and electronics of the neutral and reduced indenofluorene scaffolds. The NMR data reveal that reduction from the neutral to the dianion introduces an aromatic ring current to the formerly anti-aromatic indenofluorene, as evidenced by the nearly 1 ppm downfield shift of the proton at position 1. The X-ray data of **6b**$^{2-}$ corroborate this finding, as the localized double bonds of the central indacene moiety in **6** become essentially delocalized. Interestingly, the specific coordination of the rubidium ions has a small effect on the bond lengths of **6b**$^{2-}$, as the η^2 and η^6 X-ray structures have RMSD difference of 0.03 Å when comparing only the carbons of the IF core.

The location of the unpaired electron of the anion radical is discerned from the EPR spectrum and interpreted with the aid of calculated DFT results. This information serves as a crude first approximation for the location of the unpaired electron in the singly reduced state of **6**, for example, in an OFET device behaving as an n-channel material. Likewise, this can be a simple representation of the negatively charged IF in OPVs. Comparing the experimental results to 20 DFT methods reveals that there are several good functionals for predicting the HFCCs of the anion radical. Several functionals performed well, and the three recommended functionals for predicting HFCCs of PCHs are B97-D, B3LYP, and B3PW91, all of which gave MUEs of less than 0.32 G. There is considerable room for improvement, as errors in HFCCs of this magnitude strongly affect the appearance of the predicted spectrum. This could possibly be improved with basis sets that better describe the Kohn−Sham wave function close to the nucleus, such as EPR-III, which is currently not available for silicon and thus not explored.[73]

Additionally, the NMR chemical shift prediction for the neutral species revealed that B3PW91, BP86, PW91, PBE, and B3LYP gave MUEs of less than 0.1 ppm for the ^{1}H NMR spectrum. The ^{1}H NMR spectrum of the dianion had PBE, PW91, B3LYP, BP86, τ-HCTH, B97-D, and BLYP yield MUEs within 0.1 ppm of the experimental values. The neutral ^{13}C NMR spectrum had four functionals with MUEs within 5 ppm of experimental values: M06-L, B3LYP, τ-HCTH, and B97-D. The ^{13}C spectrum of the dianion had PW91, PBE, BP86, B3LYP, B97-D, and τ-HCTH within 5 ppm; thus, for NMR spectral prediction for PCHs, the recommendation would be either the B3LYP or τ-HCTH functional.

The absorbance transition energy prediction of the functionals was clear for the neutral and anion radical species; however, for the dianion, the interpretation of calculated results was much more ambiguous, with large disagreements between the functionals used. For the neutral species and anion radical, ωB97X-D, CAM-B3LYP, and BHandHLYP all gave results in close agreement to experimental data. The DFT-calculated absorbance transition energies for the dianion were in general poor, and the only functional that seems appropriate for this is PBE0, as the other functionals that were close to the experimental value gave unclear results.

Overall, it is quite remarkable how close the computed values are, considering that all of the calculations were completed for a

dx.doi.org/10.1021/ja503870z | J. Am. Chem. Soc. 2014, 136, 9181−9189

single gas-phase molecule. This study is an indicator that currently available DFT methods can be used for prediction of spectral properties of PCHs with reasonable accuracy and can thus be used for guiding synthesis in developing new PCHs with desired properties. Unfortunately, there does not appear to be one DFT method used in this study that gives results clearly in better agreement with experiment relative to the other methods considered, and the DFT methods must be chosen on a case-by-case basis.

■ ASSOCIATED CONTENT

Supporting Information

Experimental procedures, computational details and xyz coordinates, copies of spectra, and X-ray CIF files for **6a** and **6b**$^{2-}$. This material is available free of charge via the Internet at http://pubs.acs.org.

■ AUTHOR INFORMATION

Corresponding Author

haley@uoregon.edu

Notes

The authors declare no competing financial interest.

■ ACKNOWLEDGMENTS

We thank the National Science Foundation (CHE-1013032 and CHE-1301485 to M.M.H.; CHE-1212441 to M.A.P.) for support of this research as well as for support in the form of instrumentation (CHE-0923589) and computer grants (OCI-0960354) at UO. S.J.P. acknowledges the ACS-PRF (51677-UR4) for support. B.D.R. acknowledges the American Chemical Society Division of Organic Chemistry for an Emmanuil Troyanski Fellowship as well as a National Science Foundation GK-12 Fellowship (DGE-0742540). We thank Dr. Daniel T. Chase for providing X-ray-quality crystals of **6a**.

■ REFERENCES

(1) Harvey, R. G. *Polycyclic Aromatic Hydrocarbons*; Wiley-VCH: Weinheim, Germany, 1997.

(2) *Introduction to Organic Electronic and Optoelectronic Materials and Devices*; Sun, S.-S., Dalton, L. R., Eds.; CRC Press: Boca Raton, FL, 2008.

(3) Anthony, J. E. *Angew. Chem., Int. Ed.* **2008**, *47*, 452−483.

(4) Seyler, H.; Purushothaman, B.; Jones, D. J.; Holmes, A. B.; Wong, W. W. H. *Pure Appl. Chem.* **2012**, *84*, 1047−1067.

(5) Bunz, U. H. F.; Engelhart, J. U.; Lindner, B. D.; Schaffroth, M. *Angew. Chem., Int. Ed.* **2013**, *52*, 3810−3821.

(6) Niimi, K.; Shinamura, S.; Osaka, I.; Miyazaki, E.; Takimiya, K. *J. Am. Chem. Soc.* **2011**, *133*, 8732−8739.

(7) Kawase, T.; Fujiwara, T.; Kitamura, C.; Konishi, A.; Hirao, Y.; Matsumoto, K.; Kurata, H.; Kubo, T.; Shinamura, S.; Mori, H.; Miyazaki, E.; Takimiya, K. *Angew. Chem., Int. Ed.* **2010**, *49*, 7728−7732.

(8) Fix, A. G.; Chase, D. T.; Haley, M. M. *Top. Curr. Chem.* **2012**, DOI: 10.1007/128_2012_376.

(9) Zhou, Q.; Carroll, P. J.; Swager, T. M. *J. Org. Chem.* **1994**, *59*, 1294−1301.

(10) Reisch, H.; Wiesler, U.; Scherf, U.; Tuytuylkov, N. *Macromolecules* **1996**, *29*, 8204−8210.

(11) Hafner, K.; Stowasser, B.; Krimmer, H.-P.; Fischer, S.; Böhm, M. C.; Lindner, H. J. *Angew. Chem., Int. Ed.* **1986**, *25*, 630−632.

(12) Chase, D. T.; Rose, B. D.; McClintock, S. P.; Zakharov, L. N.; Haley, M. M. *Angew. Chem., Int. Ed.* **2011**, *50*, 1127−1130.

(13) Chase, D. T.; Fix, A. G.; Rose, B. D.; Weber, C. D.; Nobusue, S.; Stockwell, C. E.; Zakharov, L. N.; Lonergan, M. C.; Haley, M. M. *Angew. Chem., Int. Ed.* **2011**, *50*, 11103−11106.

(14) Kendrick, M. J.; Neunzert, A.; Payne, M. M.; Purushothaman, B.; Rose, B. D.; Anthony, J. E.; Haley, M. M.; Ostroverkhova, O. *J. Phys. Chem. C* **2012**, *116*, 18108−18116.

(15) Chase, D. T.; Fix, A. G.; Kang, S. J.; Rose, B. D.; Weber, C. D.; Zhong, Y.; Zakharov, L. N.; Lonergan, M. C.; Nuckolls, C.; Haley, M. M. *J. Am. Chem. Soc.* **2012**, *134*, 10349−10352.

(16) Nishida, J.; Tsukaguchi, S.; Yamashita, Y. *Chem.—Eur. J.* **2012**, *18*, 8964−8970.

(17) Bachmann, R.; Gerson, F.; Gescheidt, G.; Hafner, K. *Magn. Reson. Chem.* **1995**, *33*, S60−S65.

(18) Cary, D. R.; Green, J. C.; O'Hare, D. *Angew. Chem., Int. Ed. Engl.* **1997**, *36*, 2618−2620.

(19) Coropceanu, V.; Cornil, J.; Da, S. F.; Olivier, Y.; Silbey, R.; Bredas, J.-L. *Chem. Rev.* **2007**, *107*, 926−952.

(20) Hachmann, J.; Olivares-Amaya, R.; Atahan-Evrenk, S.; Amador-Bedolla, C.; Sanchez-Carrera, R. S.; Gold-Parker, A.; Vogt, L.; Brockway, A. M.; Aspuru-Guzik, A. *J. Phys. Chem. Lett.* **2011**, *2*, 2241−2251.

(21) Cramer, C. J. *Essentials of Computational Chemistry: Theories and Models*; John Wiley & Sons Ltd.: Chichester, UK, 2002; pp 249−303.

(22) Staroverov, V. N.; Scuseria, G. E.; Tao, J.; Perdew, J. P. *J. Chem. Phys.* **2003**, *119*, 12129−12137.

(23) Schreckenbach, G.; Ziegler, T. *Theor. Chem. Acc.* **1998**, *99*, 71−82.

(24) Helgaker, T.; Jaszunski, M.; Ruud, K. *Chem. Rev.* **1999**, *99*, 293−352.

(25) Filatov, A. S.; Zabula, A. V.; Spisak, S. N.; Rogachev, A. Yu.; Petrukhina, M. A. *Angew. Chem., Int. Ed.* **2014**, *53*, 140−145.

(26) Hermosilla, L.; Calle, P.; Garcia de la Vega, J. M.; Sieiro, C. *J. Phys. Chem. A* **2005**, *109*, 1114−1124.

(27) Barone, V.; Crescenzi, O.; Improta, R. *Quant. Struct.-Act. Relat.* **2002**, *21*, 105−118.

(28) Jacquemin, D.; Wathelet, V.; Perpete, E. A.; Adamo, C. *J. Chem. Theory Comput.* **2009**, *5*, 2420−2435.

(29) Adamo, C.; Jacquemin, D. *Chem. Soc. Rev.* **2013**, *42*, 845−856.

(30) Coulson, C. A. *Tetrahedron* **1961**, *12*, 193−195.

(31) Marcel Swart's Website. DFT2012. http://www.marcelswart.eu/ (accessed April 7, 2014).

(32) Becke, A. D. *Phys. Rev. A: Gen. Phys.* **1988**, *38*, 3098−3100.

(33) Perdew, J. P. *Phys. Rev. B* **1986**, *33*, 8822−8824.

(34) Perdew, J. P.; Burke, K.; Ernzerhof, M. *Phys. Rev. Lett.* **1996**, *77*, 3865−3868.

(35) Perdew, J. P.; Chevary, J. A.; Vosko, S. H.; Jackson, K. A.; Pederson, M. R.; Singh, D. J.; Fiolhais, C. *Phys. Rev. B: Condens. Matter* **1992**, *46*, 6671−6687.

(36) Becke, A. D. *J. Chem. Phys.* **1993**, *98*, 1372−1377.

(37) Becke, A. D. *J. Chem. Phys.* **1993**, *98*, 5648−5652.

(38) Stephens, P. J.; Devlin, F. J.; Chabalowski, C. F.; Frisch, M. J. *J. Chem. Phys.* **1994**, *98*, 11623−11627.

(39) Heyd, J.; Scuseria, G. E.; Ernzerhof, M. *J. Chem. Phys.* **2003**, *118*, 8207−8215.

(40) Paier, J.; Marsman, M.; Hummer, K.; Kresse, G.; Gerber, I. C.; Angyan, J. G. *J. Chem. Phys.* **2006**, *125*, 249901/1−249901/2.

(41) Heyd, J.; Scuseria, G. E.; Ernzerhof, M. *J. Chem. Phys.* **2006**, *124*, 219906/1.

(42) Perdew, J. P.; Ernzerhof, M.; Burke, K. *J. Chem. Phys.* **1996**, *105*, 9982−9985.

(43) Ernzerhof, M.; Scuseria, G. E. *J. Chem. Phys.* **1999**, *110*, 5029−5036.

(44) Adamo, C.; Barone, V. *J. Chem. Phys.* **1999**, *110*, 6158−6170.

(45) Adamo, C.; Barone, V. *J. Chem. Phys.* **1998**, *108*, 664−675.

(46) Zhao, Y.; Truhlar, D. G. *Theor. Chem. Acc.* **2008**, *120*, 215−241.

(47) Zhao, Y.; Truhlar, D. G. *J. Chem. Phys.* **2006**, *125*, 194101/1−194101/18.

(48) Zhao, Y.; Schultz, N. E.; Truhlar, D. G. *J. Chem. Phys.* **2005**, *123*, 161103/1−161103/4.

(49) Zhao, Y.; Schultz, N. E.; Truhlar, D. G. *J. Chem. Theory Comput.* **2006**, *2*, 364−382.

(50) Boese, A. D.; Handy, N. C. *J. Chem. Phys.* **2002**, *116*, 9559−9569.
(51) Grimme, S. *J. Comput. Chem.* **2006**, *27*, 1787−1799.
(52) Chai, J.-D.; Head-Gordon, M. *J. Chem. Phys.* **2008**, *128*, 084106/1−084106/15.
(53) Chai, J.-D.; Head-Gordon, M. *Phys. Chem. Chem. Phys.* **2008**, *10*, 6615−6620.
(54) Vydrov, O. A.; Scuseria, G. E. *J. Chem. Phys.* **2006**, *125*, 234109/1−234109/9.
(55) Vydrov, O. A.; Heyd, J.; Krukau, A. V.; Scuseria, G. E. *J. Chem. Phys.* **2006**, *125*, 074106/1−074106/9.
(56) Vydrov, O. A.; Scuseria, G. E.; Perdew, J. P. *J. Chem. Phys.* **2007**, *126*, 154109/1−154109/9.
(57) Yanai, T.; Tew, D. P.; Handy, N. C. *Chem. Phys. Lett.* **2004**, *393*, 51−57.
(58) Frisch, M. J.; Trucks, G. W.; Schlegel, H. B.; Scuseria, G. E.; Robb, M. A.; Cheeseman, J. R.; Scalmani, G.; Barone, V.; Mennucci, B.; Petersson, G. A.; Nakatsuji, H.; Caricato, M.; Li, X.; Hratchian, H. P.; Izmaylov, A. F.; Bloino, J.; Zheng, G.; Sonnenberg, J. L.; Hada, M.; Ehara, M.; Toyota, K.; Fukuda, R.; Hasegawa, J.; Ishida, M.; Nakajima, T.; Honda, Y.; Kitao, O.; Nakai, H.; Vreven, T.; Montgomery, J. A., Jr.; Peralta, J. E.; Ogliaro, F.; Bearpark, M.; Heyd, J. J.; Brothers, E.; Kudin, K. N.; Staroverov, V. N.; Kobayashi, R.; Normand, J.; Raghavachari, K.; Rendell, A.; Burant, J. C.; Iyengar, S. S.; Tomasi, J.; Cossi, M.; Rega, N.; Millam, N. J.; Klene, M.; Knox, J. E.; Cross, J. B.; Bakken, V.; Adamo, C.; Jaramillo, J.; Gomperts, R.; Stratmann, R. E.; Yazyev, O.; Austin, A. J.; Cammi, R.; Pomelli, C.; Ochterski, J. W.; Martin, R. L.; Morokuma, K.; Zakrzewski, V. G.; Voth, G. A.; Salvador, P.; Dannenberg, J. J.; Dapprich, S.; Daniels, A. D.; Farkas, Ö.; Foresman, J. B.; Ortiz, J. V.; Cioslowski, J.; Fox, D. J. *Gaussian 09*, Revision C.01; Gaussian Inc.: Wallingford, CT, 2010.
(59) Rose, B. D.; Chase, D. T.; Weber, C. D.; Zakharov, L. N.; Lonergan, M. C.; Haley, M. M. *Org. Lett.* **2011**, *13*, 2106−2109.
(60) Rose, B. D.; Zakharov, L. N.; Haley, M. M. *Acta Crystallogr., Sect. E: Struct. Rep. Online* **2013**, *69*, o890.
(61) Zabula, A. V.; Sumner, N. J.; Filatov, A. S.; Spisak, S. N.; Grigoryants, V. M.; Petrukhina, M. A. *Eur. J. Inorg. Chem.* **2012**, 4675−4683.
(62) Spisak, S. N.; Sumner, N. J.; Zabula, A. V.; Filatov, A. S.; Rogachev, A. Yu.; Petrukhina, M. A. *Organometallics* **2013**, *32*, 3773−3779.
(63) Zabula, A. V.; Spisak, S. N.; Filatov, A. S.; Grigoryants, V. M.; Petrukhina, M. A. *Chem.—Eur. J.* **2012**, *18*, 6476−6484.
(64) Neander, S.; Tio, F. E.; Buschmann, R.; Behrens, U.; Olbrich, F. *J. Organomet. Chem.* **1999**, *582*, 58−65.
(65) Green, J. R.; Dunbar, R. C. *J. Phys. Chem. A* **2011**, *115*, 4968−4975.
(66) Rellan-Pineiro, M.; Rodriguez-Otero, J.; Cabaleiro-Lago, E. M.; Josa, D. *J. Mol. Modeling* **2013**, *19*, 2049−2055.
(67) Hassan, A.; Dinadayalane, T. C.; Grabowski, S. J.; Leszczynski, J. *Phys. Chem. Chem. Phys.* **2013**, *15*, 20839−20856.
(68) Spisak, S. N.; Zabula, A. V.; Filatov, A. S.; Rogachev, A. Yu.; Petrukhina, M. A. *Angew. Chem., Int. Ed.* **2011**, *50*, 8090−8094.
(69) Dunitz, J. D.; Kruger, C.; Irngartinger, H.; Wang, M.; Nixdorf, M. *Angew. Chem., Int. Ed.* **1988**, *27*, 387−389.
(70) Treitel, N.; Shenhar, R.; Aprahamian, I.; Sheradsky, T.; Rabinovitz, M. *Phys. Chem. Chem. Phys.* **2004**, *6*, 1113−1121.
(71) Stoll, S.; Schweiger, A. *J. Magn. Reson.* **2006**, *178*, 42−55.
(72) *MATLAB*; The MathWorks, Inc..
(73) Barone, V. In *Recent Advances in Density Functional Methods*; Chong, D., Ed.; World Scientific: Singapore, 1995; pp 287−334.
(74) Liu, T.; Troisi, A. *Adv. Mater.* **2013**, *25*, 1038−1041.
(75) Klessinger, M.; Michl, J. *Excited States and Photochemistry of Organic Molecules*; VCH: New York, 1995; pp 34−36.
(76) Charaf-Eddin, A.; Planchat, A.; Mennucci, B.; Adamo, C.; Jacquemin, D. *J. Chem. Theory Comput.* **2013**, *9*, 2749−2760.